PNAS RESEARCH ARTICLE | MICROBIOLOGY OPEN ACCESS

Antibiotic perseverance increases the risk of resistance development

Gerrit Brandis[a,1], Jimmy Larsson[a], and Johan Elf[a,1]

Edited by Fernando Baquero, Ramón y Cajal University Hospital, IRYCIS, Madrid, Spain; received September 23, 2022; accepted December 7, 2022 by Editorial Board Member Richard P. Novick

Preprint: A preprint of this article has been published on BioRxiv, https://doi.org/10.1101/2022.09.20.508757.

The rise of antibiotic-resistant bacterial infections poses a global threat. Antibiotic resistance development is generally studied in batch cultures which conceals the heterogeneity in cellular responses. Using single-cell imaging, we studied the growth response of *Escherichia coli* to sub-inhibitory and inhibitory concentrations of nine antibiotics. We found that the heterogeneity in growth increases more than what is expected from growth rate reduction for three out of the nine antibiotics tested. For two antibiotics (rifampicin and nitrofurantoin), we found that sub-populations were able to maintain growth at lethal antibiotic concentrations for up to 10 generations. This perseverance of growth increased the population size and led to an up to 40-fold increase in the frequency of antibiotic resistance mutations in gram-negative and gram-positive species. We conclude that antibiotic perseverance is a common phenomenon that has the potential to impact antibiotic resistance development across pathogenic bacteria.

cellular heterogeneity | mutation frequency | single-cell microscopy | rifampicin | antibiotic resistance evolution

Significance

Antibiotics are a crucial part of modern medicine. The treatment of bacteria with antibiotic concentrations above the minimal inhibitory concentration leads to growth arrest or cell death. Here, we show that the cells within populations of supposably identical bacterial clones are not equally affected by exposure to the antibiotics rifampicin and nitrofurantoin. While all cells within the population cease to grow eventually, a sub-population of cells can maintain growth for up to 10 generations. This perseverance of growth increased the risk of antibiotic resistance development by up to 40-fold in gram-negative and gram-positive species. Our findings suggest that antibiotic perseverance is a common phenomenon across pathogenic bacteria that has the potential to impact antibiotic resistance development.

The rise in antibiotic-resistant bacterial infections is a global threat to modern medical health care. The dispersal of multi-drug-resistant pathogens is driven by the acquisition of chromosomal mutations and mobile genetic elements (1, 2). The standard model of resistance development divides selective conditions into "sub-MIC" selection below the minimal inhibitory concentration (MIC) and "above-MIC" selections above the MIC (3). Sensitive populations cannot grow during selection above the MIC which makes the existence of preexisting mutations or resistance elements essential for the development of resistance (4). Contrarily, sub-MIC selection conditions permit the growth of sensitive bacteria, and de novo resistance can arise during replication. The resistant population has a growth advantage and can outcompete the sensitive parental population (5, 6). Additionally, sub-MIC concentrations of antibiotics can increase conjugation frequencies, select for populations that carry a multi-drug resistance plasmid, and increase bacterial swimming motility as well as biofilm formation (7–10). Although there are notable exceptions (11–14), studies on the effect of antibiotics on bacterial growth have generally been performed in batch cultures with large populations thus overlooking any cell-to-cell heterogeneity in the response to antibiotic exposure. Here, we systematically exposed *Escherichia coli* to sub-MIC and MIC concentrations of nine distinct antibiotics and used time-lapse microscopy to analyze the bacterial growth response on a single-cell level. Our main aims were i) to measure cell-to-cell heterogeneity in growth response as a function of antibiotic concentration, and ii) to determine how this heterogeneity affects antibiotic resistance development.

Results

We selected nine distinct antibiotics that cover a wide variety of antibiotic classes and targets, and determined their MIC in Lysogeny broth (LB) with 425 mg/L Pluronics (Fig. 1*A* and *SI Appendix*, Table S1). We then exposed *E. coli* cells to antibiotic concentrations corresponding to 1/8×, 1/4×, 1/2×, and 1× MIC (*SI Appendix*, Table S2) in a modified version of the mother-machine microfluidic chip (15) that enabled simultaneous measurements at all four antibiotic concentrations (Fig. 1*B*). Each microfluidic experiment was divided into three stages: i) the pre-exposure stage (1 h) where cells were grown in LB to determine the baseline growth rate; ii) the exposure stage (4 h) where the growth media contained antibiotics; and iii) the post-exposure stage (3 h) where the growth medium was switched back to antibiotic-free LB to test if the cells were able to recover from the antibiotic exposure (Fig. 1*C*). Using time-lapse phase-contrast microscopy and automated image analysis, we were able to measure the growth rates of thousands of individual cells during each experiment

Author contributions: G.B. and J.E. designed research; G.B. and J.L. performed research; J.E. contributed new reagents/analytic tools; G.B. analyzed data; and G.B., J.L., and J.E. wrote the paper.

The authors declare no competing interest.

This article is a PNAS Direct Submission. F.B. is a guest editor invited by the Editorial Board.

[1]To whom correspondence may be addressed. Email: gerrit.brandis@icm.uu.se or johan.elf@icm.uu.se.

This article contains supporting information online at https://www.pnas.org/lookup/suppl/doi:10.1073/pnas.2216216120/-/DCSupplemental.

Published January 3, 2023.

(Fig. 1 *D* and *E* and *SI Appendix*, Figs. S1–S3). We found that for all nine antibiotics, the cell-to-cell heterogeneity, measured as coefficient of variation (CV) of the growth rates for the growing cells, increased as a function of antibiotic concentration and antibiotic exposure time (Fig. 2 and *SI Appendix*, Fig. S4). Since the growth heterogeneity increased similarly for all nine antibiotics, we tested if this was a general effect caused by the reduction in growth rate rather than the specific action of the antibiotics. We performed a microfluidic experiment where we changed the medium from LB to minimal medium with different carbon sources (to mimic the average growth rate for different antibiotic concentrations) (*SI Appendix*, Fig. S5). The results showed that the reduction in growth rate caused a significant increase in cell-to-cell heterogeneity that could account for the observed effects in six out of the nine antibiotics [chloramphenicol (CHL), ciprofloxacin (CIP), nitrofurantoin (NIT), rifampicin (RIF), spectinomycin (SPT), and tetracycline (TET)]. The increase in growth heterogeneity of the remaining antibiotics [carbenicillin (CAR), ceftriaxone (CRO), and gentamycin (GEN)] was greater than expected from growth rate reduction (Fig. 2 and *SI Appendix*, Fig. S6). Next, we focused on the last 30 min of growth during the 1× MIC exposure phase where the effect of the antibiotics is expected to be the strongest and analyzed the distribution of growth rates of all cells during this window (Fig. 3). While most antibiotics displayed a unimodal distribution of growth rates around a single average value, nitrofurantoin and rifampicin showed a bimodal distribution. Here, we observed a split between a dead main population and a surviving sub-population that maintained growth with a reduced relative growth rate indicating strong cell-to-cell heterogeneity (Fig. 3 *F* and *G*). For these two antibiotics, the increase in growth heterogeneity was not identified to be greater than expected from growth rate reduction (Fig. 2 and *SI Appendix*, Fig. S6). In both cases, the split into two populations appeared too late during the antibiotic exposure phase (NIT) or included a sub-population that was too small (RIF) to affect the overall growth heterogeneity above the level that was expected from growth rate reduction (Fig. 3).

To further investigate the observed bimodal distribution, we focused our analysis on the sub-population that maintained growth in the presence of rifampicin. Rifampicin is commonly used to determine mutation rates (16, 17), and the mutations that cause rifampicin resistance are well understood (18, 19). A deeper analysis of the growth behavior of the cells during rifampicin exposure showed that the sub-population that maintained growth displayed specific phenotypic changes: i) the cells were actively dividing with a growth rate of approximately half the growth rate in LB, and ii) the cell shape changed to slimmer cells. These changes in phenotype were maintained in the daughter cells and fully reverted to the wild-type state within a couple of hours after removal of the antibiotic (Fig. 3 *G* and *J*). To test if the growing sub-population had an increased MIC, we repeated the experiment but increased the antibiotic exposure time to 17 h. As before, we could observe the growing sub-population but after approximately 7 h of antibiotic exposure, all growth had ceased, indicating that the sub-population did not have an increased MIC value but rather a reduction of growth inhibition (*SI Appendix*, Fig. S7*B*). We also performed an equivalent experiment with a high concentration of rifampicin (~6× MIC) and found no growing sub-population, further confirming that no MIC increase is involved in

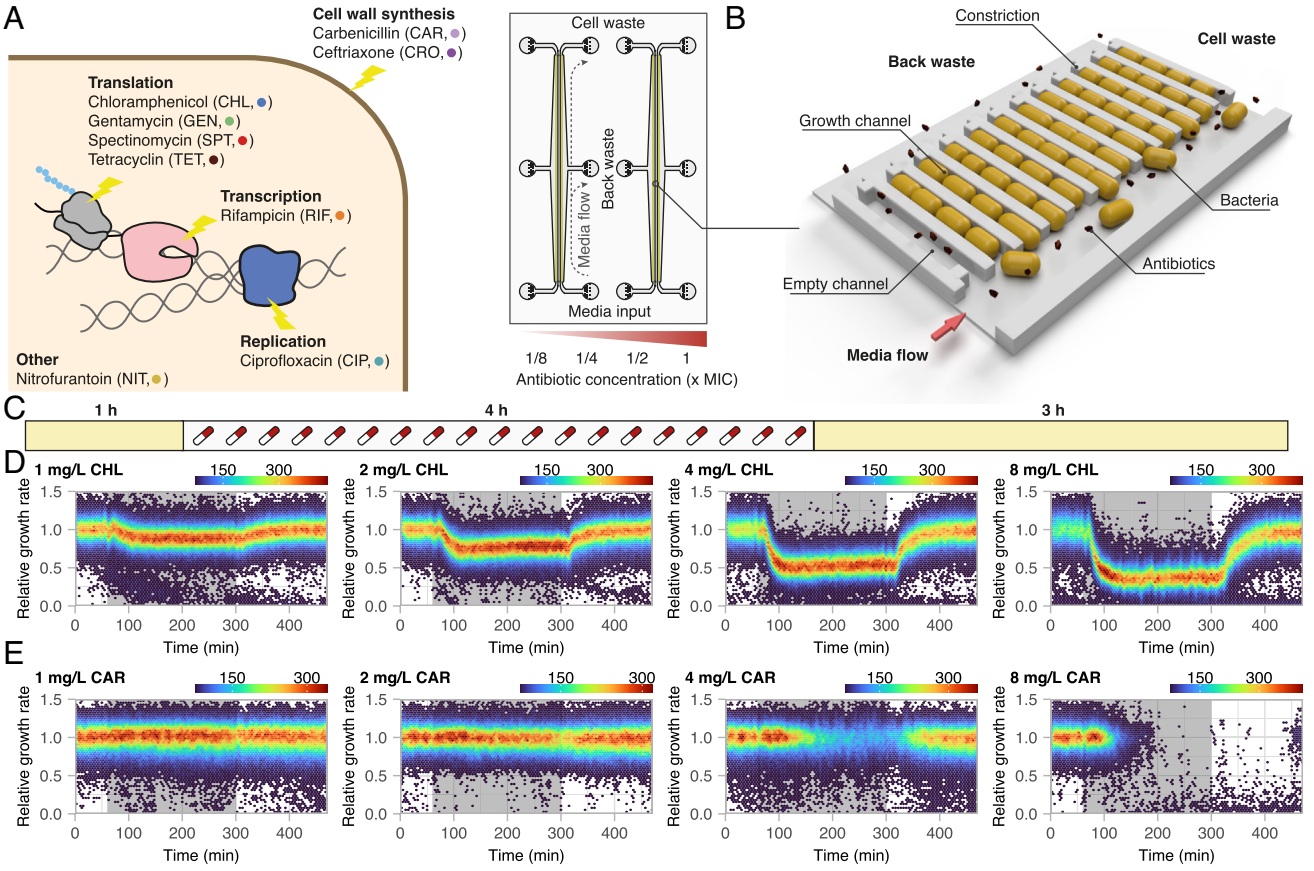

Fig. 1. Overview of antibiotic exposure experiment. (*A*) Antibiotics used in the study. (*B*) Schematic overview of the microfluidic setup. (*C*) Timeline of the microfluidic experiments defined by growth in LB (yellow) or LB supplemented with antibiotics (gray). (*D* and *E*) Relative growth rates of single cells during the antibiotic exposure experiment. The antibiotic exposure phase is indicated by the gray background. Displayed are representative examples of a bacteriostatic (*D*) and a bactericidal (*E*) antibiotic. See *SI Appendix*, Figs. S1–S3 for all experiments.

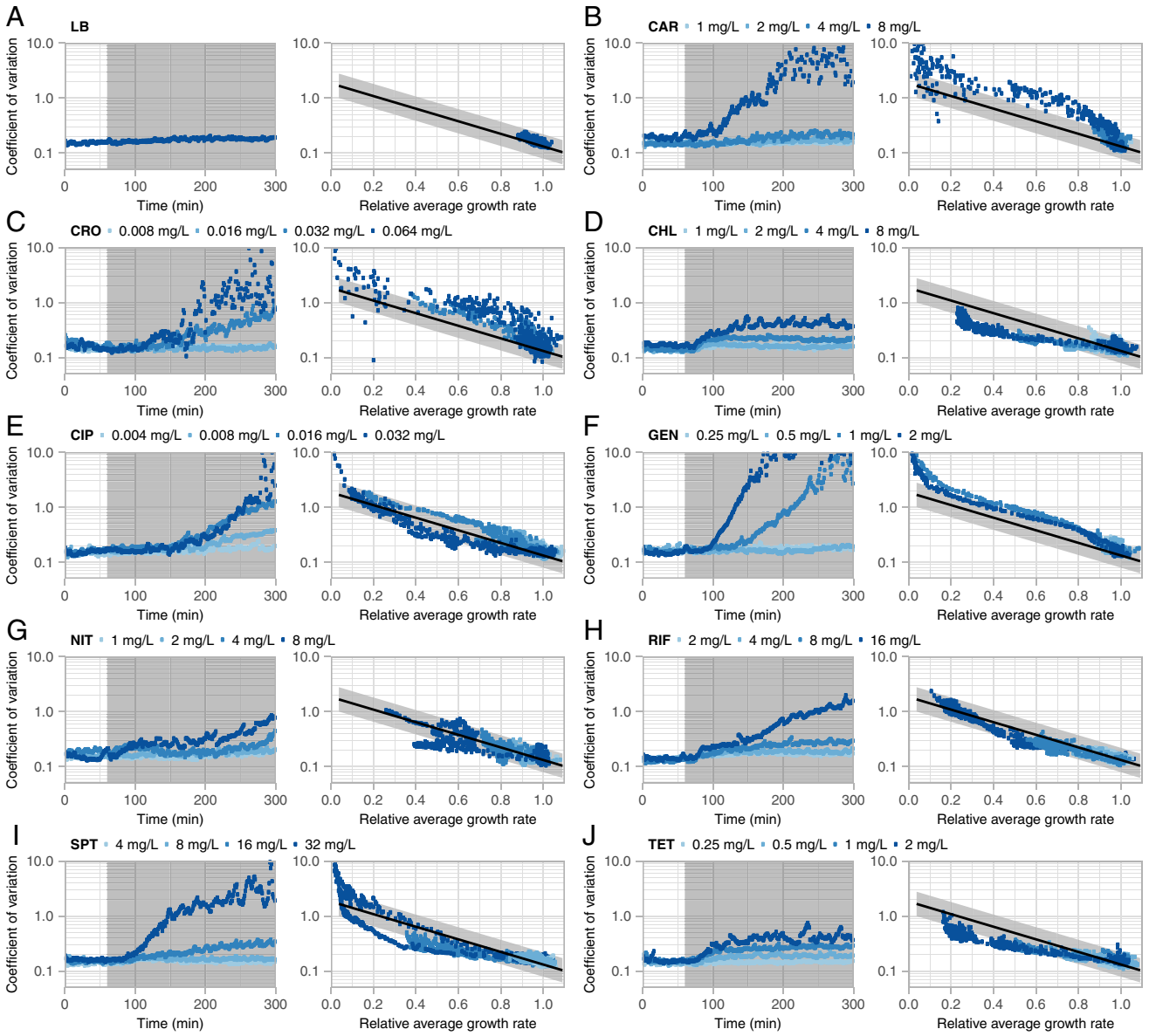

Fig. 2. Antibiotic exposure increases cell-to-cell heterogeneity. (*A–J*) Cell-to-cell growth heterogeneity, measured as CV. (*Left*) As function of antibiotic exposure time. The period of antibiotic exposure is indicated by the gray background. (*Right*) As function of relative average growth rate. The black line and gray area indicate cell-to-cell heterogeneity that is expected from growth rate reduction (*SI Appendix*, Fig. S5). The dots correspond to the CV of all single-cell growth rates at a given timepoint. Depicted are the combined results from two independent experiments for which the single cell data is pooled per time point. See *SI Appendix*, Figs. S4 and S6 for the results of each individual experiment.

the observed phenotype (*SI Appendix*, Fig. S7*C*). Due to the lack of MIC increase, we conclude that the observed phenotype cannot be classified as antibiotic resistance or heteroresistance (20). Our data show that the cells are actively dividing during antibiotic exposure, which excludes antibiotic persistence, and antibiotic tolerance is a general attribute of each cell in the population rather than of a sub-population (21, 22). Thus, we conclude that the observed phenotype cannot be properly described by either of these terms and therefore refer to it as antibiotic perseverance within this work. We define the term antibiotic perseverance as the phenotypic property of a sub-population to maintain active replication for a significantly longer time than the main population in the presence of an inhibitory concentration of antibiotics. The perseverance phenotype can be detected by the bimodal distribution of single-cell growth rates within the population during a transient period after antibiotic exposure.

To quantify the frequency of antibiotic perseverance within the bacterial population, we determined the number of cell divisions of all mother cells within the 17 h exposure experiment (*SI Appendix*, Fig. S7). We found that high-level rifampicin exposure (~6× MIC) led to a rapid halt of cell division (1.1 ± 0.4 cell divisions). Low-level rifampicin exposure (1× MIC), on the other hand, resulted in a slower termination of growth (3.8 ± 1.2 cell divisions) with a significantly broader cell-to-cell variation based on the SDs of the distributions [$P < 0.001$, two-sided Kolmogorov–Smirnov (KS) test] (Fig. 4*A*). The persevering sub-population (fraction of cells that grew more than twice the number of generations than the average) represented 2% of the mother cells and displayed a 2.6-fold increase in the number of cell divisions compared to the main population (9.5 ± 0.6 vs. 3.7 ± 0.9 cell divisions). Furthermore, the growth rate of the persevering mother cells was indistinguishable from that of the main population before the antibiotic treatment ($P = 0.65$, two-sided t test) (Fig. 4*B*).

To determine the impact of antibiotic perseverance on the bacterial population, we estimated the change in population size after antibiotic exposure at low-level and high-level rifampicin based on

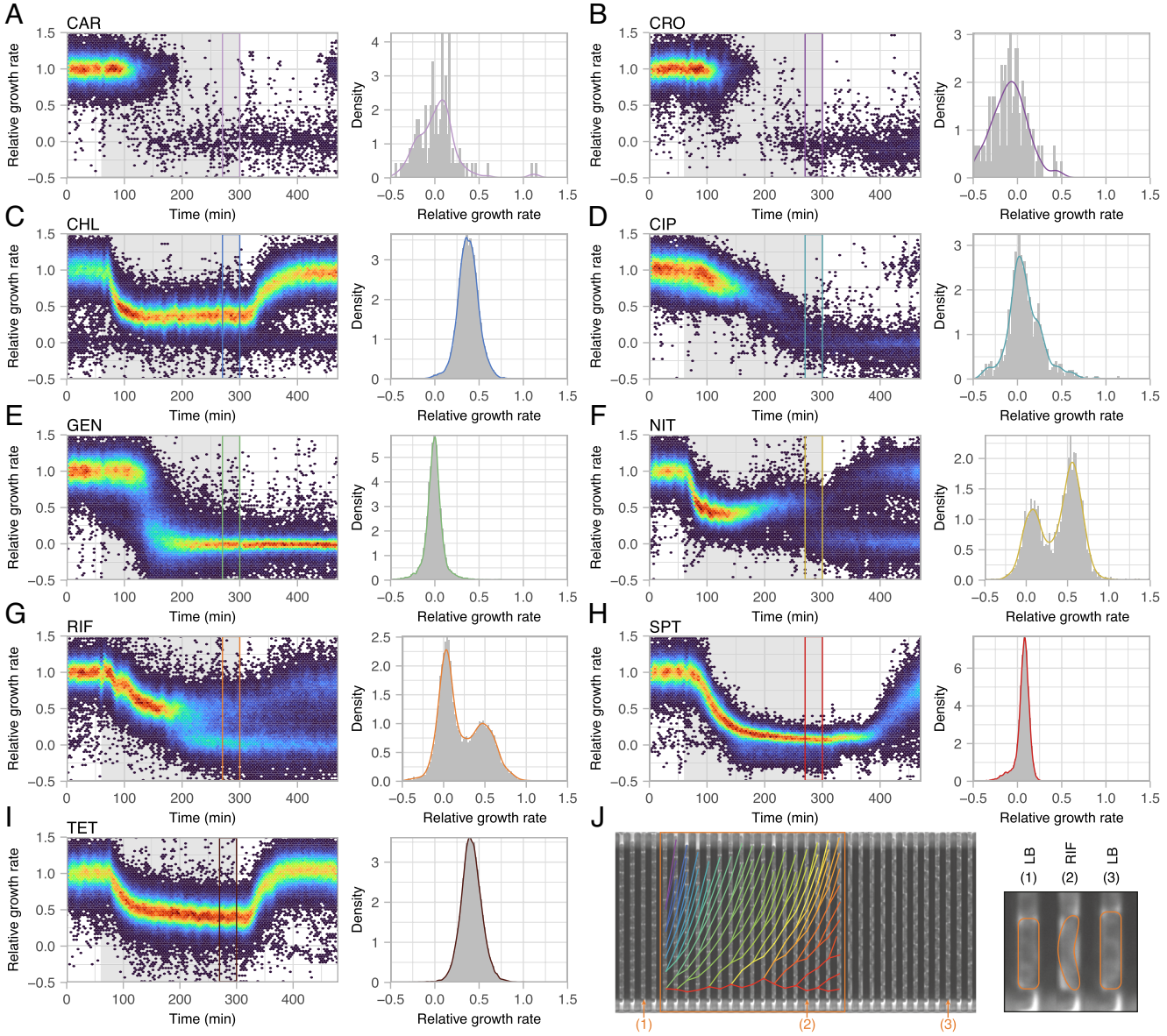

Fig. 3. Antibiotic perseverance observed during growth in nitrofurantoin and rifampicin. (*A–I*, *Left*) Distribution of single-cell growth rates as a function of time during the microfluidic experiments. The antibiotic exposure phase is indicated by the gray background. (*Right*) Density plot of the single-cell growth rates during the last 30 min of antibiotic exposure as indicated by the box in to the left. (*J*) Time-lapse images (every 15 min) of a channel that maintains growth in the experiment displayed in panel *G*. The phase of antibiotic exposure is indicated by the orange box. The change of position of each cell between images is indicated during the antibiotic exposure phase, and branches in the connection lines correspond to cell divisions. The shape of the mother cell during the different phases of the experiment is displayed to the right.

the distributions of cell divisions obtained in the 17 h exposure experiment. The total population size increased 14-fold during low-level exposure compared to high-level rifampicin concentrations (31.3-fold vs. 2.2-fold). Importantly, half of the difference (51%) was caused by the 2% of cells that displayed antibiotic perseverance demonstrating that this phenotype can have a significant impact on the bacterial population during antibiotic exposure (Fig. 4*C*).

Every round of replication can lead to the spontaneous formation of a mutation that could decrease the susceptibility of the resulting strain to the antibiotic (4, 23). Thus, sub-populations that maintain growth during lethal selection conditions could increase the risk of antibiotic resistance development. We tested this hypothesis by selecting high-level rifampicin-resistant mutants during exposure to low-level and high-level concentrations of rifampicin and found an 8.3-fold increase in mutation frequency during low-level rifampicin concentrations ($P = 0.008$, two-sided *t* test) (Fig. 4 *D* and *E*). This increase in mutation frequency disappeared when adjusting for the increase in population size ($P = 0.11$, two-sided *t* test). Thus, the increased mutation frequency can be fully accounted for with the observed growth during these selection conditions. Next, we tested if the observed mutations indeed appeared after antibiotic exposure, as expected from the perseverance phenotype, by analyzing which rifampicin resistance mutations were selected during low-level and high-level antibiotic exposure. The mutation analysis showed that i) both selection conditions resulted in single amino-acid changes within the *rpoB* gene that encodes the β-subunit of RNA polymerase, and ii) the mutations found during the low-level selection conditions were not preexisting within the population but must have occurred during the antibiotic exposure time (Fig. 4 *G–M* and *SI Appendix*, Table S3). Furthermore, we confirmed that the mutations occurring during low-level rifampicin exposure were not

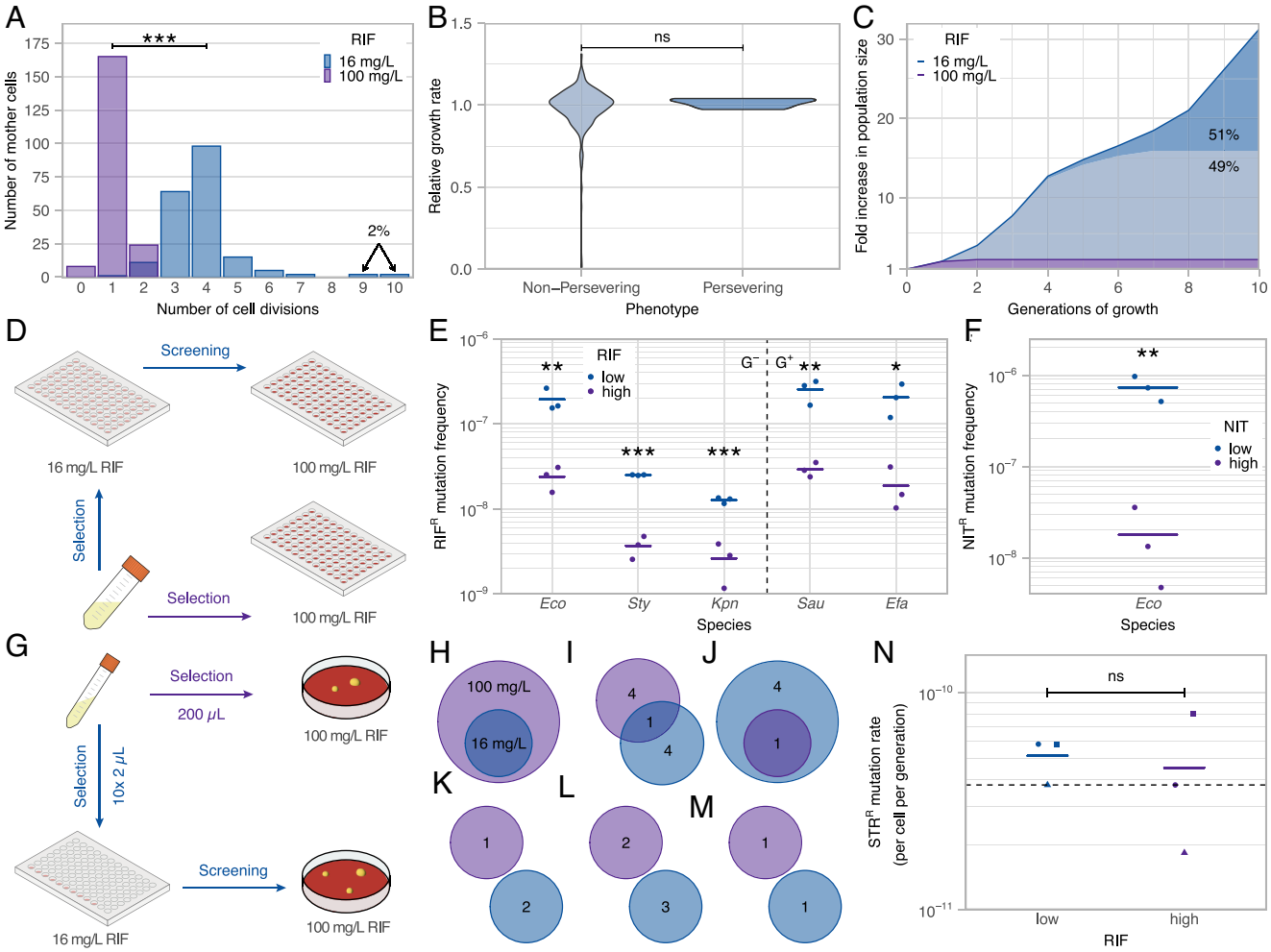

Fig. 4. Antibiotic perseverance increases population size and frequency of antibiotic resistance development. (*A*) Distribution of cell divisions of mother cells during the 17 h rifampicin exposure experiment (two-sided KS test). (*B*) Violin plot displaying the growth rates of persevering and non-persevering mother cells before antibiotic exposure (two-sided *t* test). (*C*) Estimated change of population size after exposure to rifampicin based on the distribution of cell divisions displayed in panel *A*. (*D*) Experimental setup to determine the frequency of high-level rifampicin resistance during different selection conditions. (*E* and *F*) Mutation frequencies for high-level rifampicin (*E*) and nitrofurantoin (*F*) resistance during selection at low-level and high-level antibiotic concentrations. The line indicates the average value (two-sided *t* test). (*G*) Experimental setup to test if rifampicin resistance mutations are preexisting in the bacterial culture. (*H–M*) Venn diagrams for the null-hypothesis that all rifampicin resistance mutations are preexisting within the culture (*H*) and for rifampicin resistance mutations in the *rpoB* gene obtained in five independent experiments (*H–M*). (*N*) Mutation rate for streptomycin resistance of rifampicin-resistant mutants selected during low and high rifampicin concentrations in the experiments displayed in panels *I–M* (ns, $P > 0.05$, *$P < 0.05$, **$P < 0.01$, ***$P < 0.001$).

selected in cells with a higher intrinsic mutation rate for example due to inactivation of genes involved in the mismatch repair system (Fig. 4*N*). These results agree with the expectation that sustained growth during antibiotic exposure increases the frequency of resistance development.

To test if these results are unique to *E. coli*, we performed a 17 h rifampicin exposure experiment with *Salmonella enterica* serovar Typhimurium and found an equivalent persevering sub-population at low-level rifampicin concentrations (*SI Appendix*, Fig. S8). As before, the mutation frequency for high-level rifampicin resistance was significantly increased (6.8-fold, $P = 0.002$, two-sided *t* test) during exposure to low-level compared to high-level rifampicin concentrations (Fig. 4*E* and *SI Appendix*, Table S4). We also found significant increases in mutation frequency of similar magnitude in all other tested gram-negative (*Klebsiella pneumoniae*) and gram-positive (*Enterobacter faecalis*, *Staphylococcus aureus*) species, indicating that the observed phenomenon is common across pathogenic bacteria (Fig. 4*E* and *SI Appendix*, Table S4). Finally, we tested the mutation frequency for nitrofurantoin resistance in *E. coli* since we also observed a bimodal distribution of growth rates in the presence of nitrofurantoin (Fig. 3*F*). The results showed that the mutation frequency for nitrofurantoin resistance was increased 40.2-fold when selected at low-level concentration of nitrofurantoin compared to direct selection at the high-level concentration ($P = 0.005$, two-sided *t* test) (Fig. 4*F*).

Discussion

Previous research has shown that heteroresistance, persistence, and tolerance can significantly contribute to the development of antibiotic resistance (20, 24, 25). Our data describe an additional phenotype that appears to be common among pathogenic bacteria and applies to at least two antibiotics (rifampicin and nitrofurantoin). The frequency of perseverance (~2% of cells), the lack of MIC increase, and the reversible phenotype indicate that this phenotype is not caused by stable genetic changes (26). The persevering bacterial cells change growth rate and shape during antibiotic exposure, and this phenotype reverts quickly after the removal of the antibiotics which could indicate a changed state of gene expression within the cells. Intrinsic cell-to-cell variability within bacterial populations has been demonstrated for multiple resistance-related genes such as efflux pumps and stress response

regulators (13, 27). Rifampicin and nitrofurantoin differ with regard to molecular mass (823 Da vs. 238 Da), mechanism of action (inhibition of transcription vs. DNA damage), and genes involved in resistance development (*rpoB* vs. *nfsAB*) (18, 28). Thus, it is unlikely that heterogeneity in the expression of identical genes cause the perseverance phenotype of these two drugs but not to any of the other seven that were included in this study. Among the tested antibiotics, rifampicin has the largest molecular mass (RIF: 823 Da, others: 238 to 581 Da), has difficulties to penetrate the bacterial outer membrane, and is the only antibiotic that targets the RNA polymerase (29, 30). It is possible that gene expression related to permeability of the outer membrane (i.e., porin or lipopolysaccharide-related genes) reduces the uptake of rifampicin into the cell. Alternatively, increased expression of the RNA polymerase could effectively reduce the number of drug molecules per target protein. Both effects could explain why sub-populations are less sensitive to the drug. A feature that sets nitrofurantoin apart from the other antibiotics is that it needs to be activated within the bacterial cell to exhibit its antibacterial effect (31). Cell-to-cell heterogeneity in the expression of the genes that activate nitrofurantoin (*nfsA* and *nfsB*) could be responsible for the observed perseverance phenotype (28). Since activated nitrofurantoin is known to cause DNA damage, it is also possible that heterogeneity in the expression of the corresponding DNA repair enzymes is the cause of the perseverance (31). Independent of the precise mechanism, the resulting perseverance phenotype enables extended survival and growth during short-term antibiotic exposure (~7 h in our experiments with rifampicin) and increases the frequency of antibiotic resistance mutations for both antibiotics. While we have only studied the selection of chromosomal mutations during this growth phase, it is likely that growth under these conditions also increases the risk of conjugational transfer of multi-resistance plasmids or acquisition of resistance genes by transduction or transformation. The condition that we find drives resistance development for a subset of antibiotics, i.e., sub-MIC-level antibiotic concentrations, are present in the environment when it's polluted by antibiotics or when antibiotic treatments are prematurely terminated. In this way, insights from single-cell biology are important to drive antibiotic stewardship policies.

Materials and Methods

Bacterial Strains and Growth Conditions. A list of bacterial strains used in this study can be found in *SI Appendix*, Table S5. Bacteria were grown at 37 °C in LB broth with surfactant Pluronic F-109 (Sigma-Aldrich 542342, 425 mg/L) or on plates of LB broth solidified with 1.5% agar (LA plates). Antibiotics were added to the media as described. When indicated, bacteria were grown in defined minimal medium (M9) with surfactant Pluronic F-109 (425 mg/L) and enriched with 0.2% glucose, 0.2% glycerol, and 0.08% RPMI 1640 amino acids (Sigma Aldrich R7131) as described.

Antibiotics. All antibiotics were ordered from Sigma Aldrich. Stock solutions were prepared in water for carbenicillin (C1389), ceftriaxone (C5793), ciprofloxacin (PHR1044), gentamycin (G1914), and spectinomycin (S4014), in 70% ethanol for chloramphenicol (C0378) and tetracycline (T7660), in methanol for rifampicin (R3501), and in dimethyl sulfoxide for nitrofurantoin (46502).

MIC. The MICs were determined by broth dilution in 96-well plates. Bacterial colonies were resuspended in 0.9% NaCl to 0.5 McFarland and diluted 100-fold in growth medium. In total, 50 µL cells were added to each well with 50 µL antibiotic solution resulting in a total volume of 100 µL per well containing approximately 10^5 cfu bacterial cells (10^6 cfu/mL). The microtiter plates were sealed and incubated for 18 h at 37 °C before reading. All MIC tests were performed in three biological replicates. A list of the tested antibiotic concentration ranges and MIC results can be found in *SI Appendix*, Table S6.

Time Kill Assay. Approximately 10^6 cfu of exponentially growing cells were added into 2 mL pre-warmed LB with Pluronics containing antibiotics at 8× MIC (~5×10^5 cfu/mL) and incubated shaking at 37 °C. After 0, 1, 2, and 4 h, samples were taken, diluted in 0.9% NaCl, and plated on LA plates. Plates were incubated overnight at 37 °C after which colonies were counted. Bactericidal activity was defined as >99% reduction of the initial inoculum size.

Determination of Mutation Frequency to High-Level Rifampicin and Nitrofurantoin Resistance. Overnight cultures were diluted in fresh LB with Pluronics and rifampicin/nitrofurantoin, and aliquots of 100 µL were distributed in the wells of a 96-well microtiter plate. See *SI Appendix*, Tables S4 and S7 for details on the antibiotic concentrations and inoculum sizes for the different species. A dilution series of each overnight culture was plated on LA plated to determine the actual inoculation size for each well. The 96-well plates were sealed and incubated for ~18 h shaking at 37 °C, and LA plates were incubated for ~18 h at 37 °C. From each positive well, 1 µL culture was transferred into 100 µL fresh media containing the high antibiotic concentration to confirm high-level resistance. Plates were sealed and incubated for ~18 h shaking at 37 °C before growth was determined. Mutation frequencies were calculated by dividing the number of positive wells by the combined bacterial inoculation size within the 96-well plate. All measurements were performed in biological triplicates, and frequencies of resistance development at low and high antibiotic concentrations were compared using a two-sided two-sample *t* test.

Determination of Mutation Rate to Streptomycin Resistance. The mutation rate to streptomycin resistance was used to compare the general mutation rates in rifampicin-resistant isolates. Twenty 1 mL cultures of each isolate were grown overnight shaking at 37 °C. Each culture was centrifuged for 5 min at 7,000 rpm in a benchtop centrifuge (5424 R, Eppendorf). The bacterial pellets were resuspended in approximately 100 µL LB, plated on LA plates containing 100 mg/L streptomycin, and incubated overnight at 37 °C. Mutation rates were calculated according to the formula

$$\mu = -\left(\frac{1}{N}\right)\ln(P0), \qquad [1]$$

where µ is the mutation rate, N is the number of viable cells per plate (~2.8×10^9 cfu), and P0 is the proportion of plates that did not give rise to streptomycin-resistant colonies. A chi-squared test based on the number of cultures with and without streptomycin-resistant colonies was used to compare the results from the rifampicin-resistant isolates with wild-type *E. coli*. The results of the assay are shown in *SI Appendix*, Table S8.

Test for Preexisting Mutations. Five independent cultures of 1 mL LB with Pluronics were inoculated and grown overnight shaking at 37 °C. From each overnight culture, 200 µL were plated on LA plates supplemented with 425 mg/L Pluronics and 100 mg/L rifampicin, and 10 wells of a 96-well microtiter plate containing 100 µL LB supplemented with Pluronics and 16 mg/L rifampicin were inoculated with 2 µL culture each (in total 20 µL overnight culture) (Fig. 4*G*). All colonies on the plates containing 100 mg/L rifampicin were restreaked on the same selective plates and mutations within the *rpoB* gene were identified by local sequencing. From each positive well, 10 µL culture was plated on LA supplemented with Pluronics and 100 mg/L rifampicin and incubated overnight at 37 °C. One colony per plate was restreaked on the same selective media followed by identification of mutations within the *rpoB* gene by local sequencing. For each of the five independent cultures, the types of mutations isolated from selections at 100 mg/L rifampicin were compared to the mutations isolated from selections using 16 mg/L rifampicin (Fig. 4 *I*–*M* and *SI Appendix*, Table S3). The null hypothesis for preexisting mutations was that the mutations from 16 mg/L rifampicin should be a subset of the mutations from 100 mg/L rifampicin due to the 10-fold excess of culture used in the selection for high-level rifampicin resistance (Fig. 4*H*).

PCR and Local DNA Sequencing. PCRs for local DNA sequencing were performed using 2× PCR Master mix (Thermo Scientific). The following PCR program was used: 95 °C for 3 min, 35 cycles of 95 °C for 30 s, 50 °C for 30 s, and 72 °C for 1 min, followed by 72 °C for 10 min. Local sequencing was carried out by Eurofins Genomics Europe Shared Services GmbH, Konstanz, Germany. Primer design and sequence analysis were performed using the CLC Main Workbench

21.0.3 (CLCbio, QIAGEN, Denmark). See *SI Appendix*, Table S9 for a list of oligonucleotides.

Microfluidics Experiments. Microfluidic experiments were performed using a modified version of the polydimethylsiloxane mother machine microfluidic chip previously described (15). The version of the chip permitted simultaneous measurements of four different antibiotic concentrations (Fig. 1*B*). Medium pressure was controlled using a homebuilt microfluidic flow controller.

For the microfluidic experiments, overnight cultures of cells were diluted 1,000-fold in fresh LB medium with Pluronics and grown shaking at 37 °C for 4 h before loading into the microfluidic chip. Cells were grown in the microfluidic chip for approximately 2 h before the start of the experiments.

Microscopy was performed using a Ti2-E (Nikon)-inverted microscope equipped with a CFI Plan Apochromat DM Lambda 1.45/100× objective (Nikon), a DMK 38UX304 camera (The Imaging Source), and a Spectra Gen. 1 (Lumencor) light source within a H201-ENCLOSURE hood with a H201-T-UNIT-BL controller (OKOlab). The microscope was controlled by Micro-Manager (version 1.4.23) (32) running in-house-built plugins. Phase-contrast images were acquired every minute or second minute with 80 ms exposure.

Data Analysis. Image analysis to determine single-cell growth rates was done in MATLAB (Mathworks). Microscopy data were processed using an automated analysis pipeline developed previously (33), with one exception; segmentation of phase-contrast images was done using a U-net neural network (34) trained in-house. All raw data images and analysis software are openly accessible through SciLifeLab data repository (https://doi.org/10.17044/scilifelab.21517710).

All other data analyses were performed with R 4.0.3 (35), and the results were plotted using the R package ggplot2 3.3.3 (36). Raw data and analyses scripts are available online through SciLifeLab data repository (https://doi.org/10.17044/scilifelab.21517710).

Data, Materials, and Software Availability. Raw microscopy image data and computational code used for analysis and plotting have been deposited in https://www.scilifelab.se/data/repository/ [https://doi.org/10.17044/scilifelab.21517710].

ACKNOWLEDGMENTS. We thank S. Zikrin and O. Broström for help with the image analysis. This study was made possible by grants to J.E. from the European Research Council(advanced grant no. 885360), the Swedish Foundation for Strategic Research (grant no. ARC19-0016), the Knut and Alice Wallenberg Foundation (grant no. 2016.0077, 2017.0291, and 2019.0439), and the eSSENCE e-science initiative. The computations and data management were enabled by resources provided by the Swedish National Infrastructure for Computing (SNIC) at UPPMAX, partially funded by the Swedish Research Council through grant agreement no. 2018-05973.

Author affiliations: [a]Department of Cell and Molecular Biology, Science for Life Laboratory, Uppsala University 751 24, Uppsala, Sweden

1. A. H. Holmes *et al.*, Understanding the mechanisms and drivers of antimicrobial resistance. *Lancet* **387**, 176–187 (2016).
2. N. K. Petty *et al.*, Global dissemination of a multidrug resistant *Escherichia coli* clone. *Proc. Natl. Acad. Sci. U.S.A.* **111**, 5694–5699 (2014).
3. D. Hughes, D. I. Andersson, Selection of resistance at lethal and non-lethal antibiotic concentrations. *Curr. Opin. Microbiol.* **15**, 555–560 (2012).
4. S. E. Luria, M. Delbruck, Mutations of bacteria from virus sensitivity to virus resistance. *Genetics* **28**, 491–511 (1943).
5. E. Gullberg *et al.*, Selection of resistant bacteria at very low antibiotic concentrations. *PLoS Pathog.* **7**, e1002158 (2011).
6. E. Wistrand-Yuen *et al.*, Evolution of high-level resistance during low-level antibiotic exposure. *Nat. Commun.* **9**, 1599 (2018).
7. E. Gullberg, L. M. Albrecht, C. Karlsson, L. Sandegren, D. I. Andersson, Selection of a multidrug resistance plasmid by sublethal levels of antibiotics and heavy metals. *mBio* **5**, e01918-01914 (2014).
8. E. Shun-Mei *et al.*, Sub-inhibitory concentrations of fluoroquinolones increase conjugation frequency. *Microb. Pathog.* **114**, 57–62 (2018).
9. I. C. Stanton, A. K. Murray, L. Zhang, J. Snape, W. H. Gaze, Evolution of antibiotic resistance at low antibiotic concentrations including selection below the minimal selective concentration. *Commun. Biol.* **3**, 467 (2020).
10. S. Westhoff *et al.*, The evolution of no-cost resistance at sub-MIC concentrations of streptomycin in *Streptomyces coelicolor*. *ISME J.* **11**, 1168–1178 (2017).
11. N. Q. Balaban, J. Merrin, R. Chait, L. Kowalik, S. Leibler, Bacterial persistence as a phenotypic switch. *Science* **305**, 1622–1625 (2004).
12. T. Bergmiller *et al.*, Biased partitioning of the multidrug efflux pump AcrAB-TolC underlies long-lived phenotypic heterogeneity. *Science* **356**, 311–315 (2017).
13. I. El Meouche, M. J. Dunlop, Heterogeneity in efflux pump expression predisposes antibiotic-resistant cells to mutation. *Science* **362**, 686–690 (2018).
14. I. El Meouche, Y. Siu, M. J. Dunlop, Stochastic expression of a multiple antibiotic resistance activator confers transient resistance in single cells. *Sci. Rep.* **6**, 19538 (2016).
15. O. Baltekin, A. Boucharin, E. Tano, D. I. Andersson, J. Elf, Antibiotic susceptibility testing in less than 30 min using direct single-cell imaging. *Proc. Natl. Acad. Sci. U.S.A.* **114**, 9170–9175 (2017).
16. R. Krasovec *et al.*, Mutation rate plasticity in rifampicin resistance depends on *Escherichia coli* cell-cell interactions. *Nat. Commun.* **5**, 3742 (2014).
17. M. N. Ragheb *et al.*, Inhibiting the evolution of antibiotic resistance. *Mol. Cell* **73**, 157–165.e155 (2019).
18. G. Brandis, F. Pietsch, R. Alemayehu, D. Hughes, Comprehensive phenotypic characterization of rifampicin resistance mutations in *Salmonella* provides insight into the evolution of resistance in *Mycobacterium tuberculosis*. *J. Antimicrob. Chemother.* **70**, 680–685 (2015).
19. L. Garibyan *et al.*, Use of the *rpoB* gene to determine the specificity of base substitution mutations on the *Escherichia coli* chromosome. *DNA Repair* **2**, 593–608 (2003).
20. D. I. Andersson, H. Nicoloff, K. Hjort, Mechanisms and clinical relevance of bacterial heteroresistance. *Nat. Rev. Microbiol.* **17**, 479–496 (2019).
21. N. Q. Balaban *et al.*, Definitions and guidelines for research on antibiotic persistence. *Nat. Rev. Microbiol.* **17**, 441–448 (2019).
22. A. Brauner, O. Fridman, O. Gefen, N. Q. Balaban, Distinguishing between resistance, tolerance and persistence to antibiotic treatment. *Nat. Rev. Microbiol.* **14**, 320–330 (2016).
23. B. A. Niccum, H. Lee, W. MohammedIsmail, H. Tang, P. L. Foster, The spectrum of replication errors in the absence of error correction assayed across the whole genome of *Escherichia coli*. *Genet.* **209**, 1043–1054 (2018).
24. I. Levin-Reisman, A. Brauner, I. Ronin, N. Q. Balaban, Epistasis between antibiotic tolerance, persistence, and resistance mutations. *Proc. Natl. Acad. Sci. U.S.A.* **116**, 14734–14739 (2019).
25. I. Levin-Reisman *et al.*, Antibiotic tolerance facilitates the evolution of resistance. *Science* **355**, 826–830 (2017).
26. J. Jee *et al.*, Rates and mechanisms of bacterial mutagenesis from maximum-depth sequencing. *Nature* **534**, 693–696 (2016).
27. N. M. V. Sampaio, C. M. Blassick, V. Andreani, J. B. Lugagne, M. J. Dunlop, Dynamic gene expression and growth underlie cell-to-cell heterogeneity in *Escherichia coli* stress response. *Proc. Natl. Acad. Sci. U.S.A.* **119**, e2115032119 (2022).
28. L. Sandegren, A. Lindqvist, G. Kahlmeter, D. I. Andersson, Nitrofurantoin resistance mechanism and fitness cost in *Escherichia coli*. *J. Antimicrob. Chemother.* **62**, 495–503 (2008).
29. E. A. Campbell *et al.*, Structural mechanism for rifampicin inhibition of bacterial RNA polymerase. *Cell* **104**, 901–912 (2001).
30. G. Krishnamoorthy *et al.*, Breaking the permeability barrier of *Escherichia coli* by controlled hyperporination of the outer membrane. *Antimicrob. Agents Chemother.* **60**, 7372–7381 (2016).
31. Y. Tu, D. R. McCalla, Effect of activated nitrofurans on DNA. *Biochim. Biophys. Acta* **402**, 142–149 (1975).
32. A. D. Edelstein *et al.*, Advanced methods of microscope control using muManager software. *J. Biol. Methods* **1**, e10 (2014).
33. D. Camsund *et al.*, Time-resolved imaging-based CRISPRi screening. *Nat. Methods* **17**, 86–92 (2020).
34. J. Wiktor *et al.*, RecA finds homologous DNA by reduced dimensionality search. *Nature* **597**, 426–429 (2021).
35. R Core Team, *R: A Language and Environment for Statistical Computing* (R Foundation for Statistical Computing, Vienna, Austria, 2020).
36. H. Wickham, *ggplot2: Elegant Graphics for Data Analysis* (Springer, New York, NY, 2009).